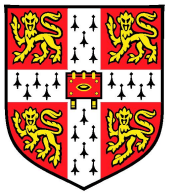

UNIVERSITY OF
CAMBRIDGE

Microfabricated z-axis vibratory rate gyroscope – A case study

Mark Nikolka
mn390@cam.ac.uk

Department of Material Science and Metallurgy
St. Edmund's College

Supervisor: Prof. Ashwin Seshia

Date of submission: March 23, 2012

1 Introduction

Micromachined gyroscopes nowadays have become an essential component in many consumer electronic devices (such as camcorders) as well as in the automotive industry (e.g. for smart breaking). Here, the practicality of microelectromechnaical (MEMS) gyroscope is originated in the fact that medium performance requirements can be met on very small areas. Nevertheless, this offers several challenges (such as high noise levels) which have to be faced during the design process. It is therefore that in the following, the design of a single-axis vibratory gyroscope is exemplary discussed addressing major difficulties that are encountered in gyroscope designs. A schematic sketch of the proposed device is shown in figure 1.

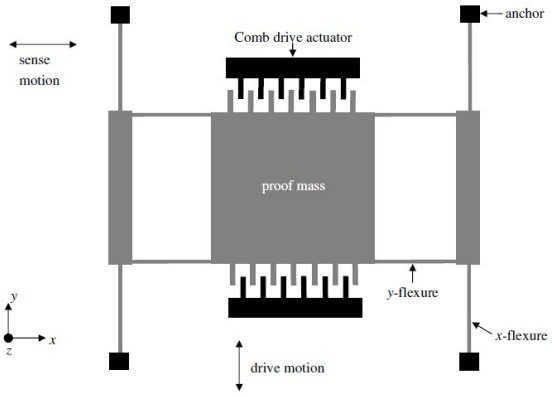

Figure 1: *Sketch of the proposed single-axis vibratory gyroscope design*

The designed device consists of a proof mass suspended by H-flexures above a substrate. Hence, the mass is free to oscillate along the y and x axis, where comb drive actuators are used to force an oscillation along the y-axis (drive direction). An applied rotation (rotation rate Ω_z) to the whole device along the z-axis, couples the drive oscillation to the sense direction (x axis) via the Coriolis effect. This oscillation subsequently is read out optically. Here, to minimize noise and thus errors in read out, the drive and sense mode frequencies are mismatched by a factor of 10 %. Thus in essence, it is the main goal of this design project, to choose the gyroscope's geometric parameters such that a minimum noise level is obtained without violating given design constraints.

2 Design Procedure

2.1 Mathematical Deviations

As a first step in the design process, the gyroscope's flexures are addressed. Here, the proof mass has to be able to oscillate in the x and y direction. This is obtained by making the suspension system compliant along the desired direction of motion and stiff in the other direction. For the given suspension type thus, the spring constants for the drive and sense direction are given by equation 1, where l,w,t are the length, width and thickness of a suspending beam and E is the Young's modulus of the beam material.

$$k_{drive} = \frac{4 \cdot E \cdot t \cdot w_d^3}{l_d^3} \quad , \quad k_{sense} = \frac{4 \cdot E \cdot t \cdot w_s^3}{l_s^3} \tag{1}$$

Once the proof mass is set into periodic oscillation by the comb drive actuators, the motion of the proof mass can be described as a two degree of freedom vibratory system. The resulting coupled differential equations are shown in equations 2 and 3 where ω denotes the resonance frequency, Q is the quality factor ($Q_i = m_i \cdot \omega_i / b_i$) and the subscript d and s denote the corresponding drive mode and sense mode components.

$$\ddot{y} \quad + \frac{\omega_d}{Q_d}\dot{y} + \omega_d^2 y = \frac{F_d}{m} sin(\omega_d t) \tag{2}$$

$$\ddot{x} \quad + \frac{\omega_s}{Q_s}\dot{x} + \omega_s^2 x + 2\Omega\dot{y} = 0 \tag{3}$$

$$\tag{4}$$

Assuming a constant drive oscillation of the form

$$y(t) \; = \; A_0 \cdot sin(\omega_d t) = \frac{Q_d \cdot F_d}{k_d} sin(\omega_d t) \tag{5}$$

the above system of differential equations can be solved for x(t), yielding the maximum displacement X shown in equation 9 (Note: Here, Mathematica was used).

$$x(t) \; = \frac{2 \cdot \Omega_z \cdot A_0 \cdot \omega_d}{\omega_s^2 \sqrt{\left(1 - \left(\frac{\omega_d}{\omega_s}\right)^2\right)^2 + \left(\frac{\omega_d}{Q_s \cdot \omega_s}\right)^2}} \cdot sin(\omega_d t - \phi) \tag{6}$$

$$\phi \quad = arctan\left(\frac{1}{Q_y\left(\frac{\omega_s}{\omega_d} - \frac{\omega_d}{\omega_s}\right)}\right) \tag{7}$$

$$x(t) \; = \frac{2 \cdot \Omega_z \cdot A_0 \cdot \omega_d \cdot C(\omega)}{\omega_s^2} \cdot sin(\omega_d t - \phi) \tag{8}$$

$$|X| \; = \frac{2 \cdot \Omega_z \cdot A_0 \cdot \omega_d}{\omega_s^2 \sqrt{\left(1 - \left(\frac{\omega_d}{\omega_s}\right)^2\right)^2 + \left(\frac{\omega_d}{Q_s \cdot \omega_s}\right)^2}} = \frac{2 \cdot \Omega_z \cdot A_0 \cdot \omega_d \cdot C(\omega)}{\omega_s^2} \tag{9}$$

From equation 9 and the expression for the gyroscope's bandwidth (at resonance) BW=ω_s/Q_s, the gyroscope's mechanical sensibility can be derived which is shown in equation 10.

$$\frac{X}{\Omega_z} = \frac{2 \cdot A_0 \cdot \omega_d \cdot C(\omega)}{\omega_s^2} = \frac{2 \cdot A_0 \cdot \omega_d \cdot C(\omega)}{BW^2 \cdot Q_s^2} \tag{10}$$

Looking at equation 10 it becomes apparent, that sensitivity and bandwidth are always subject to a trade-off. In fact for high sensitivities, an extremely narrow bandwidth (Note the inverse square dependence of sensitivity on bandwidth) is required. However here, the inverse dependence of bandwidth on the quality factor

requires e.g. vacuum packaging to reduce damping effects and consequently increase the Q factor. For a gyroscope operated under ambient conditions therefore, lower sensitivity values have to be tolerated in order to use obtainable bandwidth.

Furthermore, thermal noise is present which is caused by the Brownian force given in equation 11. By equating this force with the Coriolis induced force in the sense direction (Equation 12), an expression for the gyroscope's Brownian noise is worked out.

$$|F_{Brownian}| = \sqrt{4K_BTb_sBW} = \sqrt{\frac{4K_BT\omega_s mBW}{Q_s}} \tag{11}$$

$$|F_{coriolis}| = 2m|\dot{x}|\Omega_z = 2mA\omega_d\Omega_z \tag{12}$$

$$2mA\omega_d\Omega_z = \sqrt{\frac{4K_BT\omega_s mBW}{Q_s}} \tag{13}$$

$$\frac{\Omega_z}{\sqrt{BW}} = \sqrt{\frac{K_BT\omega_s}{mQ_sA_0^2\omega_d^2}} \tag{14}$$

As a last derivation step, the precise actuation force still remains to quantify. This is shown in equations 15 and 16 where ϵ_0 is the dielectric constant of air, U is the potential energy stored in a parallel plate capacitor, n is the number of comb fingers on each side of the substrate and g_0 is the distance (gap size) between the plates of overlap length l_0 and thickness t:

$$C = \epsilon_0\frac{A_{Overlapp}}{g_0} = \epsilon_0\frac{2\cdot n\cdot l_0\cdot t}{g_0} \tag{15}$$

$$F_d = -\nabla U = \frac{\partial C(x,y,z)}{\partial_{x,drive}}\frac{V^2}{2} = \frac{\epsilon_0\cdot n\cdot V^2\cdot t}{g_0} \tag{16}$$

In order to obtain a linearized drive force, different voltages $V_1 = V_{DC} + V_{AC}$, and $V_2 = V_{DC} - V_{AC}$ are applied to opposing sets of comb drive actuators. The resulting force thus, is given by subtracting the contribution from the top and bottom set of actuators according to equation 18.

$$F_d = \frac{\epsilon_0\cdot n\cdot V_1^2\cdot t}{w} - \frac{\epsilon_0\cdot n\cdot V_2^2\cdot t}{g_0} \tag{17}$$

$$F_d = \frac{4\cdot\epsilon_0\cdot n\cdot V_{Dc}\cdot V_{AC}\cdot t}{g_0} \tag{18}$$

3 Numerical Estimates

3.1 Flexure Design Maximizing the Drive Amplitude

From equation 14 it is apparent that for larger deflection amplitudes in the drive direction, a lower noise floor is achievable. Thus, it should be of primary interest to maximize the deflection amplitude A_0 which however, is constrained by the

maximum flexure displacement (0.02% of flexture length). Since from equation 5, the deflection amplitude is furthermore inversely proportional to the drive mode's spring constant, k_d should be minimized accordingly. Hence, using the maximum flexture length of $l_d = 500\mu$m, a beam width of w_d=2μm and the given thickness of the structual layer t = 6μm, the drive mode's minimum spring constant can be computed according to eqution 19

$$k_d = \frac{4 \cdot E \cdot t \cdot w_d^3}{l_d^3} = \frac{4 \cdot 130GPa \cdot 6\mu m \cdot (2\mu m)^3}{(500\mu m)^3} = 0.2Nm^{-1} \tag{19}$$

Subsequently using the given drive mode's resonance frequency, a value for the proof mass can be worked out according to equation 20:

$$\omega_d = \sqrt{\frac{k_d}{m}} \quad \leftrightarrow \quad m = \frac{4Etw_d^3}{l_d^3\omega_d^2} \tag{20}$$

$$m = \frac{4Etw_d^3}{l_d^3\omega_d^2} = \frac{4 \cdot 130GPa \cdot 6\mu m \cdot (2\mu m)^3}{(500\mu m)^3 \cdot (2\pi 10KHz)^2} = 5.06 \cdot 10^{-11}Kg \tag{21}$$

From the computed mass thus, the corresponding proof mass dimensions can be computed using equation 22 and 23

$$\rho_{Si} = \frac{m}{V} = \frac{m}{l_m^2 \cdot t} \quad \leftrightarrow \quad l_m = \sqrt{\frac{m}{\rho_{Si}t}} = \sqrt{\frac{4Ew_d^3}{\rho_{Si}l_d^3\omega_d^2}} \tag{22}$$

$$l_m = \sqrt{\frac{4 \cdot 130GPa \cdot (2\mu m)^3}{2400Kgm^{-3} \cdot (500\mu m)^3 \cdot (2\pi \cdot 10kHz)^2}} = 59.3\mu m \tag{23}$$

The obtained length of the (so far quadratic) proof mass is in fact too short, since the proof mass dimensions are constrained to have a minimum area of 500μm x 500μm. Therefore, the flexure dimensions have to be reiterated.

4 Reiterated Flexure Design

Looking at the equation for the Brownian noise limited resolution (equation 14) it is found, that besides a maximum drive amplitude, also a large proof mass is desired. Here however, the value of the proof mass has to be optimized, since for large masses also large actuator forces are required. Hence, the following amendments are done:

- The proof mass is assumed to be rectangular with the minimum width fixed at w_{mass}=510 μm. This value takes into account that later on, electrodes have to be fitted to the mass, slightly reducing its width.
- The corresponding length l_{mass} is maximized in order to maximize the number of electrodes which can be mounted.
- l_{mass} is selected such that the total device length (flexures + mass) remains below the maximum design length of 2mm.

Here, table 1 summarizes the selected design parameters meeting the corresponding constraints.

w_d [μm]	l_d [μm]	k_d [N/m]	m [μg]	w_{mass} [μm]	l_{mass} [μm]	A_0 [μm]
3	120	48.75	12.3	510	1681	2.4

Table 1: *Selected design parameters resulting in maximum drive amplitude*

Having selected the gyroscope's proof mass, subsequently the flexures along the sense direction can be designed according to equation 24. Here, the gyroscope's overall design width can be reduced by minimizing the sense direction's flexure length, which is achieved by choosing the minimum value for the flexure width $w_s = 2\mu$m.

$$\omega_s^2 m = \frac{4Etw_s^3}{l_s^3} \quad \leftrightarrow \quad l_s = \sqrt[3]{\frac{4Etw_s^3}{\omega_s^2 m}} = \sqrt[3]{\frac{4 \cdot 130GPa \cdot 6\mu m \cdot (2\mu m)^3}{(2\pi \cdot 11kHz)^2 \cdot 12.3\mu g}} \tag{24}$$

$$= \quad 75\mu m \tag{25}$$

Note, that the gyroscope's sense resonance frequency is higher than the drive resonance frequency which increases the gyroscope's robustness. This is due to the fact, that a small offset between the two resonance frequencies results in a controlled bandwidth of the gyroscope's dynamic response.

4.1 Actuator Force and Damping Effects

As a next step in the design process, the damping along the drive mode (and thus, the drive mode's Q−factor) shall be analyzed. For this it is assumed, that the damping is dominated by Couette flow between the proof mass and the substrate which is separated by a gap of h=2μm. Hence, the damping can be computed according to equation 26 yielding the Q−factor shown in equation 28 (Note: this value is independent of the choice of proof mass/flexure dimension).

$$b_d = \frac{\eta A_{mass}}{h} = \frac{\eta l_{mass} w_{mass}}{h} = \frac{18\mu Pas \cdot 510\mu m \cdot 1681\mu m}{2\,\mu m} \tag{26}$$

$$= 7.71 \cdot 10^{-6} kgs^{-1} \tag{27}$$

$$Q_d = \frac{m\omega_d}{b} = \frac{12.3\,\mu g \cdot 2\pi \cdot 10kHz}{7.71 \cdot 10^{-6} kgs^{-1}} = 100 \tag{28}$$

With the quality factor determined, the actuator force required for the chosen maximum displacement of A_0=2.4μm can be computed from equation 5. Furthermore, using the equation derived for the force generated by the comb drive electrodes (see equation 18), the required number of electrodes can be computed according to equation 30

$$F_d = \frac{A_0 k_d}{Q_d} = \frac{2.4\mu m \cdot 48.75 Nm^{-1}}{100} = 1.17\mu N \tag{29}$$

$$N = \frac{F_d g_0}{4\epsilon_0 t V_{AC} V_{DC}} = \frac{1.17\mu N \cdot 0.5\mu m}{4 \cdot 8.86 \cdot 10^{-12} Fm^{-1} \cdot 6\mu m \cdot 1V \cdot 10V} = 276 \tag{30}$$

The resulting number of electrodes in fact, is smaller than the total number of electrodes that fit on the proof mass, which can be shown as follows:

$$N_{max} = \frac{l_m}{(0.5+2+0.5+2)\mu m} = \frac{1681\mu m}{5\mu m} = 336 \tag{31}$$

However it also has to be considered, that comb fingers add to the damping in the drive direction which so far has been neglected. Hence, the new damping coefficient can be worked out according to equation 37 where l_0 is the overlap area which is chosen to be equivalent to the maximum displacement ($l_0 = A_0 = 2.4\mu$m) in order to minimizes damping effects.

$$b_d = \frac{\eta A_{mass}}{h} + \frac{\eta \cdot 4 \cdot n \cdot t \cdot l_0}{g_0} \tag{32}$$

Yet, this expression is dependent on n, which changes as the quality factor changes. Thus, first of all, the number of electrodes has to be recalculated taking in account the new damping conditions:

$$Q_d = \frac{\omega_d m}{\eta\left(\frac{4nA_0t}{g_0} + \frac{A_{mass}}{h}\right)} \quad , \quad A_0 = \frac{Q_d F_d}{k_d} \quad , \quad F_d = \frac{4\epsilon_0 n V_{Dc} V_{AC} t}{g_0} \tag{33}$$

$$n = \frac{g_0 A_0 k_d \eta\left(\frac{4nA_0t}{g_0} + \frac{A_{mass}}{h}\right)}{4\epsilon_0 t V_{Dc} V_{AC} \omega_d m} = \frac{g_0 A_0 k_d \eta A_{mass}}{ht(4\epsilon_0 V_{Dc} V_{AC} \omega_d m - A_0 k_d \eta 4 A_0)} \tag{34}$$

$$n = \frac{0.5\mu m \cdot 2.4\mu m \cdot 48.75 N m^{-1} \cdot \eta \cdot 8.57 \cdot 10^{-7} m^2}{2\mu m \cdot 6\mu m(4\epsilon_0 \cdot 1V \cdot 10V \cdot (\omega_d) \cdot 12.3\mu g - 4 \cdot (2.4\mu m)^2 k_d \eta)} \tag{35}$$

$$n = 296 \tag{36}$$

This obtained value for n, still is much smaller than the number of electrodes which can be fit on the proof mass. Therefore, the operational AC voltage can be reduced subsequently. Here, a value of $V_{AC} = 0.9V$ yields an electrode number of n= 332, which is selected in the following.

From this, the new damping factor is computed according to equation 37:

$$Q_d = \frac{\omega_d m}{\eta\left(\frac{4nA_0t}{g_0} + \frac{A_{mass}}{h}\right)} = \frac{2\pi \cdot 10KHz \cdot 12.3\mu g}{18\mu Pas \cdot \left(\frac{4 \cdot 332 \cdot 2.4\mu m \cdot 6\mu m}{0.5\mu m} + \frac{(510\mu m \cdot 1681\mu m}{2\mu m}\right)} = 96 \tag{37}$$

4.2 Revisited Mass Dimensions and Sense Mode Q-Factor

So far, the proof mass was assumed to be a rectangular block with massless electrodes mounted on it. This naturally is not true, since the 2n comb fingers add to the total weight of the proof mass. To account for this fact, the actuated mass is now distributed according to equation 38. Here, the length of the comb fingers (of minimum width $w_{comb} = 2\mu$m) was chosen to be 3 times the maximum displacement (A_0) in order to leave enough room for air which is squeezed out in the sense direction (Considered in the next step). The resulting proof mass area can be subsequently computed according to equation 39

$$
\begin{aligned}
m &= \rho_{Si} V_{mass} = \rho_{Si} t(w_{mass} \cdot l_{mass} + 2n \cdot 3A_0 w_{comb}) && (38)\\
l_{mass} w_{mass} &= \frac{m}{\rho_{si} t} - 2n \cdot 3 \cdot A_0 w_{comb} && (39)\\
&= \frac{12.3\mu g}{2400 kg m^{-3} \cdot 6\mu m} - 2 \cdot 332 \cdot 3 \cdot 2.4\mu m \cdot 2\mu m && (40)\\
&= 8.45 \cdot 10^{-7} m^2 && (41)\\
w_{mass} &= \frac{8.45 \cdot 10^{-7} m^2}{1681\mu m} = 504\mu m && (42)
\end{aligned}
$$

Thus according to equation 41 the proof mass width reduces to 504μm if the length is kept at its previous value.

Considering now the sense mode, the total damping can be estimated by adding the damping contribution due to Couette flow between the proof mass and the substrate, and the Squeeze Film between the comb fingers. The resulting quality factor is shown in equation 46

$$
\begin{aligned}
b_s &= \frac{\eta A_{mass}}{h} + \frac{4n \cdot 96 \cdot \eta \cdot l_0 \cdot t^3}{\pi^4 \cdot g_0^3} && (43)\\
&= \frac{18\mu Pas 510\mu m 1681\mu m}{2\mu m} + \frac{4 \cdot 332 \cdot 96 \cdot 18\mu Pas \cdot 3 \cdot 6\mu m \cdot (2.4\mu m)^3}{\pi^4 \cdot (0.5\mu m)^3} && (44)\\
&= 2.32 \cdot 10^{-5} Kgs^{-1} && (45)\\
Q_s &= \frac{m\omega_s}{b_s} = \frac{12.3\mu g \cdot (2\pi \cdot 11KHz)}{2.32 \cdot 10^{-5} Kgs^{-1}} = 37 && (46)
\end{aligned}
$$

4.3 Brownian Noise Limited Resolution and Sense Deflection

The value for the quality factor in the sense direction can subsequently be used to estimate the Brownian noise limited resolution according to equation 14

$$
\begin{aligned}
\frac{\Omega_z}{\sqrt{BW}} &= \sqrt{\frac{K_B T \omega_s}{m Q_s A_0^2 \omega_d^2}} = \sqrt{\frac{4.11 \cdot 10^{-21} J \cdot (2\pi \cdot 11kHz)}{12.3\mu 37 (2.4\mu m)^2 (2\pi \cdot 10kHz)^2}} && (47)\\
&= 1.7 \cdot 10^{-4} rad/s/\sqrt{Hz} = 0.57°/min/\sqrt{Hz} && (48)
\end{aligned}
$$

This value is much lower than the required Brownian noise limited resolution of 0.8 deg/min/$\sqrt{Hz}$. Thus, this design can be selected.

As a last step in the numerical analysis, the deflection in the sense direction has to be quantified. This is done, by inserting all device parameters into equation 9 and assuming an applied rotation rate of 1deg/s:

$$|X| = \frac{2 \cdot \left(1°/s \cdot \frac{2\pi}{360°}\right) \cdot 2.4\mu m \cdot (2\pi \cdot 10kHz)}{(2\pi \cdot \omega_s)^2 \sqrt{\left(1 - \left(\frac{10}{11}\right)^2\right)^2 + \left(\frac{10}{11 \cdot 37}\right)^2}} = 6.3 \cdot 10^{-12} m = 6.3pm \tag{49}$$

This value is extremely small, especially when comparing it to the drive mode's deflection which is shown in equation 50

$$\frac{|X|}{|Y|}/\Omega_z = \frac{6.3pm}{2.4\mu m}/1°/s = 2.6ppm/°/s \tag{50}$$

Hence, coupling of the drive oscillation into the Coriolis induced oscillation make the device readout very vulnerable. For real devices this means, that the sense mode and the drive mode have to be entirely decoupled which requires a minimization of fabrication imperfections. This way it has to be made sure, that the measured oscillation is not overwhelmed by the drive mode oscillation.

4.4 Objectives for Real Gyroscopes

In actual practice, the gyroscope has to meet a number of additional objectives. Here, for instance the sensing of small displacements has to be recorded very reliably requiring a sophisticated optical or electrical read out mechanism (e.g. by sensing actuators). At the same time, the device has to operate over a long lifetime which requires constant performance over several years. These requirements in fact, are directly tied to the obtainable accuracy of the fabrication process. In this context for instance, fluctuations in the fabrication process (e.g. due to over etching or inaccuracy of the lithography process) can cause major fluctuation in frequency matching (originated in variations of the spring constants) rendering the device non-operational.

5 Device Improvements

In order to improve the design of the z-axis rotation rate gyroscope, the device's symmetry could be improved. This in fact could reduce the coupling between the sense mode and drive mode resonance frequencies. For this, the overall drive voltage has be slightly increased which allows to use a quadratic mass instead of the required rectangular proof mass element. Nevertheless, this inevitably increases power consumption which for mobile applications is undesirable and thus, symmetry and power consumption will be subject to a trade off for the chosen MEMS design. Additionally it could be considered to improve the device's design by including a self test region into the device, which tests if an induced Coriolis force measurement meets predetermined criteria. Hence, this allows to test the device's functionality for large scale applications.

At this point it should be furthermore noted, that during the design process many effects (such as damping) have been crudely approximated. Therefore, numerical simulations and modeling of the different domains (e.g. electronics, mechanics,

electrostatics, thermodynamics) should be used, to accurately estimate the future device performance. This way, numerical simulations can be used to compare modeled device characteristics with actual device performance, which is important to understand the operation of the device and additionally identify inaccuracies in the fabrication process. Hence for future devices, imperfection sources can be included in the MEMS simulation allowing to evaluate the manufacturability of a selected MEMS designs.

Using the simulation methods described above, the gyroscope's design can be further improved. Here for instance, the device's future performance could be improved, by using a 4DOF gyroscope design, which relaxes the need for mode matching by utilizing a 2-DOF drive-direction oscillator and a 2-DOF sense-direction oscillator and thus, incorporating three proof masses into the system's design. This way, the corresponding performance of the drive mode and the sense mode can be tuned separately, which allows more room for design enhancements.

References

[1] H. Xie, G. K. Fedder, "integrated Microelectromechanical Gyroscopes", J. Aerospace Engineering, Vol. 16, No. 2, April, 2003